metals

MDPI

Article

Structural Parameter Optimization for Large Spacing Sublevel Caving in Chengchao Iron Mine

Yuye Tan [1,2,*], Mochuan Guo [1,2,*], Yimin Hao [1,2], Chi Zhang [1,2] and Weidong Song [1,2]

[1] School of Civil and Resource Engineering, University of Science and Technology Beijing, Beijing 100083, China; luobiha435@163.com (Y.H.); zhangchi9531@163.com (C.Z.); songwd@ustb.edu.cn (W.S.)
[2] Key Laboratory of Efficient Mining and Safety of Metal Mines, Ministry of Education, Beijing 100083, China
* Correspondence: tanyuye@ustb.edu.cn (Y.T.); guomochuan@163.com (M.G.)

Abstract: Non-pillar sublevel caving is beginning to use large structural parameters in China. Appropriate structural parameters can effectively control the loss and dilution of stope and improve ore drawing efficiency. In this study, taking Chengchao Iron Mine as the engineering background, a theoretical calculation, a numerical simulation, and physical similarity experiments were combined to optimize sublevel height, production drift spacing, and drawing space. The optimal structural parameter range, based on the ellipsoid ore drawing theory, was obtained as a theoretical reference for subsequent studies. A "two-step" strategy was used, in which PFC2D software (Itasca Consulting Group, Minneapolis, MN, USA) was used to numerically simulate 20 groups of different sublevel heights and production drift spacing parameters were used to determine the appropriate sublevel height and production drift spacing for the project. Subsequently, the optimization of the ore drawing space was studied using PFC3D (Itasca Consulting Group, Minneapolis, MN, USA) particle unit software, numerical simulation analysis, and similar physical experiments. The results showed that safe and efficient mining can be achieved when the structural parameters of the stope are 17.5 m sublevel height, 20 m production drift spacing, and 6 m drawing space. The findings of this study can further the goal of green and efficient mining, and provide a theoretical reference for the popularization and application of pillarless sublevel caving with large structural parameters at home and abroad. It is an effective measure for the green mining of caving mines.

Keywords: sublevel caving; numerical simulation; physical model; structural parameter; green mining

Citation: Tan, Y.; Guo, M.; Hao, Y.; Zhang, C.; Song, W. Structural Parameter Optimization for Large Spacing Sublevel Caving in Chengchao Iron Mine. *Metals* **2021**, *11*, 1619. https://doi.org/10.3390/met11101619

Academic Editor: Lijie Guo

Received: 14 September 2021
Accepted: 5 October 2021
Published: 12 October 2021

1. Introduction

Non-pillar sublevel caving offers the advantages of simple operation, high-intensity mining, high mechanization degree, safety and reliability, and relatively low mining costs [1–4]. Therefore, it has been widely used in ore mining at home and abroad [5]. The purpose of mining is to discharge ore under the overburden, leading to a large loss coefficient and dilution ratio [6,7]. Many scholars at home and abroad have conducted in-depth research on reducing loss and dilution. They have successively proposed various ore drawing theories, including ore drawing ellipsoidal and stochastic medium drawing theories [8]. These theories have been widely applied to guide the production of mines in sublevel caving [9].

The three important parameters used in sublevel caving are sublevel height, production drift spacing, and drawing space. Several researchers have studied the adjustment and optimization of mine parameters and mining management to control the recovery effect. Kvapil, R., et al. [10] optimized structural parameters through laboratory experiments on similar materials. Janelle, I. and Kvapil, R. [11] performed an experimental field study on a prototype size based on tracer recovery. David, J., et al. [12] conducted a numerical simulation experiment based on ore drawing theory. These studies focused on the flow principle of ore and rock particles [13]. For the optimization principle of structural parameters, the

difference between recovery and dilution rates in the actual production of mines is used as the criterion for determining the optimal structural parameters. In particular, high recovery and low dilution rates indicate large differences and a good recovery effect [14].

Because the structural parameters of the sublevel caving mining method can directly affect the ore recovery ratio and recovery efficiency, and then affect the overall technical and economic indicators and benefits of the mine, many scholars use different methods to optimize the structural parameters of sublevel caving stope [15,16]. To determine the appropriate stope structural parameters for the sublevel caving method, Wu et al. [17] compared and analyzed nine different stope structural parameters by laboratory test and computer numerical simulation. Zhao et al. [18] obtained the optimal structural parameters of an iron ore stope through a single-ore drawing experiment and MATLAB software (MathWorks, Natick, MA, USA) fitting analysis, combined with industrial eccentricity. Using the three ore drawing methods, the no-dilution caving method, the low-dilution caving method, the and the current cutoff caving method under large structural parameters, similar simulation experiments and PFC2D (Particle Flow Code 2D) (Itasca Consulting Group, Minneapolis, MN, USA) are used to simulate ore recovery and rock mixing. The optimal caving step of the three ore drawing methods was obtained by Jin et al. [19]. An improved flow diversion drawing technology can reduce the ore loss rate and dilution ratio [20].

In this study, the exploitation of the Chengchao Iron Mine through sublevel caving without a sill pillar was used as the engineering background. The range of optimal structure parameters was calculated based on ellipsoid drawing theory and the intersection degree of the drawn-out orebody, and a "two-step" strategy was adopted. PFC2D software (Itasca Consulting Group, Minneapolis, MN, USA) simulated the sublevel caving with different sublevel heights and production drift spacing to determine the optimal solution while maintaining the existing drawing space. Next, PFC3D three-dimensional discrete element software (Itasca Consulting Group, Minneapolis, MN, USA) was used to adopt the finite difference method. Combined with the physical ore drawing similar simulation experiment [21,22] and theoretical calculation results with the experimental model ratio of 1:100, and considering the relationship between drawing step and ore loss and dilution, the optimal drawing step was determined by mutual verification from the numerical simulation, physical experiment, and theoretical analysis [23].

2. Theoretical Calculation of Optimal Structural Parameters

At present, the generally accepted criterion for determining the optimal structural parameters of sublevel caving without a sill pillar is that "the morphology of the caving body should be consistent with that of the drawn-out ore body". Jin et al. [24] modified this criterion, where the optimization of structural parameters refers to optimizing the spatial arrangement of the drawn-out ore body, and the degree of compaction is the best. Theoretically, the drawn-out ore body can be divided into two equivalent and optimal arrangements: high sublevel and large space. The arrangement of large space is advantageous [25] considering mines' current technical equipment conditions in China, as shown in Figure 1.

The relationship between sublevel height and production drift spacing is expressed as:

$$\frac{H}{B} = \frac{\sqrt{3}}{6}\frac{a}{b} \tag{1}$$

$$\frac{L}{H} = \frac{(1+\sin\theta)(c+\cos\theta)}{2a} \tag{2}$$

In this equation, H is the sublevel height, m; B is the production drift spacing, m; a is the long axis of the discharged ellipsoid, m; b is the short axis of the discharged ellipsoid, m; L is the step distance of the ore drawing, m; θ is the included angle (2°–4°, θ = 2°) between the long axis of the quasi-ellipsoid and the end wall; c is the short semiaxis of the quasi-ellipsoid in the direction of vertical access, m.

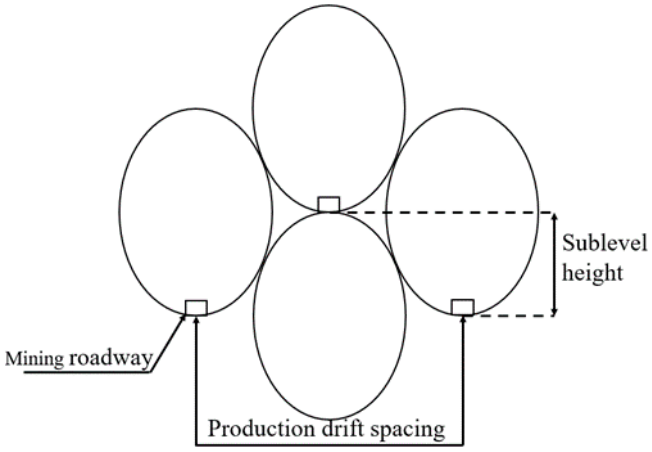

Figure 1. Arrangement of large space of discharged ellipsoid.

In actual ore drawing, the morphology change of the drawn-out ore body is dynamic, and its actual morphology is close to that of Figure 2. Chengchao Iron Mine adopts low dilution ore drawing of sublevel caving without a sill pillar. The optimal structural parameters [26] can be theoretically determined, including the sublevel height, production drift spacing, and the interval of caved ore, based on the geometric relation of the optimal spatial arrangement of the discharged ellipsoid.

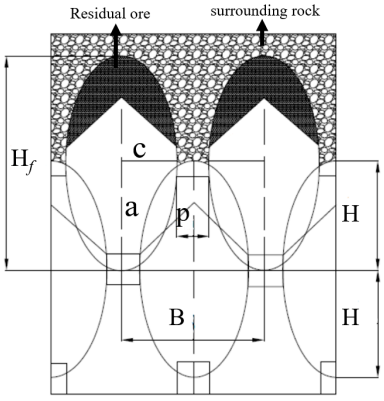

Figure 2. The ellipsoid arrangement is released in the direction of the vertical access.

According to the drawing theory, the drawn-out ore body is a quasi-ellipsoid, and its size can be determined by the a, b, and c axes of the ellipsoid. The ellipsoidal arrangement in Figure 2 allows as much ore to be recovered as possible and can be expressed in the vertical direction as follows:

$$B = 2c + p \tag{3}$$

$$H_f = 2H = 2a \tag{4}$$

In this equation, H_f is the ellipsoid discharge height, m; p is the access width, m.

The caving step L can be determined through geometric analysis, using the following equation:

$$L = b\cos\theta + a\sin\theta \tag{5}$$

The eccentricity of the ellipsoid is expressed as:

$$b = a\sqrt{1 - {\varepsilon_b}^2} \tag{6}$$

$$c = a\sqrt{1 - {\varepsilon_c}^2} \tag{7}$$

According to the actual situation of the mine, at the level of −500~−570 m, the sublevel height H is 17.5 m, that is, a = 17.5 m, and the access width p = 3.8 m, through the industrial experiment eccentricity, ε_b = 0.95, ε_c = 0.90. These values are substituted in Equations (6) and (7) to yield b = 5.46 m and c = 7.62 m. Next, the production drift spacing B_1 is 18.91 m by substituting the values of a and b into Equation (1). Production drift spacing B_2 is 19.04 m by substituting the values of b and c into Equation (3). Thus, the theoretical production drift spacing ranges from 18.91 m to 19.04 m. The interval of caved ore L_1 is 4.46 m by substituting a, c, and θ into Equation (2), and the interval of caved ore L_2 is 6.07 m by substituting a, b, and θ into Equation (5). Therefore, the interval of caved ore ranges is 4.46~6.07 m.

3. PFC Numerical Simulation Study

3.1. Optimization of Sublevel Height and Production Drift Spacing

3.1.1. Simulation Scheme

Sublevel caving without a sill pillar was adopted for the mining stage −500~−570 m in Chengchao Iron Mine. The ore body was about 1500 m long and 296° in the overall strike; the direction of dip was 214°, the amount of inclination was 0°–45°, and the average thickness was 72.95 m. The ore body mainly comprised marble, with good stability. The mine production scale was 3.4 million t/a, and the ore geological grade was 48%. The sublevel height was 17.5 m, and the production drift spacing was 15 m. Compared with the advanced level at home and abroad, the stope structure parameters can be optimized. Through PFC2D (Itasca Consulting Group, Minneapolis, MN, USA), the numerical simulation was carried out with sublevel heights of 17.5 m, 19 m, 21 m, 23.5 m, and 26 m, and production drift spacing of 15 m, 18 m, 20 m, and 22 m to study the influence of sublevel height and production drift spacing on ore recovery and dilution index.

In this study, the vertical production drift direction profile was selected to establish a calculation model. An ore drawing scheme, with a sublevel height of 21 m and production drift spacing of 20 m, was taken as an example, as shown in Figure 3a. The model's width was 60 m, its height was 126 m, the upper overburden was 42 m, the lower ore body was 84 m (four sublevels), and the edge angle of the middle and deep holes was 60°. The equivalent radius R of the ore unit in the model was 200 mm, and the equivalent radius R of the overburden unit was 300 mm, using a volume equivalent method. Gravity ore dropping was adopted to make the corresponding collapsed ore move under the action of gravity.

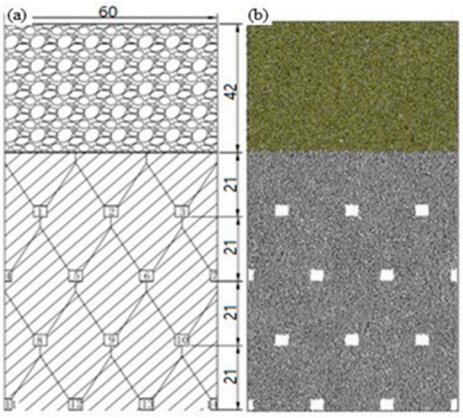

Figure 3. Schematic of the model: (**a**) schematic of model size, m; (**b**) 2D numerical model diagram.

A total of 41,331 balls are found in the model, where 35,093 red balls represent the ore, and 6238 yellow balls represent the waste rock. The particle unit diagram of the 2D numerical simulation of the ore drawing scheme is shown in Figure 3b.

PFC2D modeling requires debugging micromechanical parameters. The micromechanical parameters assumed by the model are first assigned to conduct numerical tests and

then are matched with the macro test parameters obtained from laboratory tests to enable continuous debugging. These micromechanical parameters can be applied to the numerical calculation when the calculated results are consistent with the laboratory test results [26,27]. The size of the 3D ore drawing numerical model adopted in this study was consistent with the laboratory test, and the contact-stiffness model was adopted for the particle interaction model. The modeling parameters of this model mainly included ore and rock particle radius, normal stiffness, shear stiffness, friction coefficient, density, and color [28,29]. The micromechanical parameters in Table 1 are consistent with the macroscopic mechanical parameters after repeated debugging.

Table 1. Micromechanical parameters of the model.

Particle Type	Average Particle Size/m	Normal Stiffness/N·m^{-1}	Tangential Stiffness/N·m^{-1}	Friction Coefficient	Density/ kg·m^{-3}	Color
Ore	0.2	1.2×10^8	1.2×10^8	0.1	4000	Red
rock	0.3	1.0×10^8	1.0×10^8	0.2	2700	yellow

Before ore drawing, the cutoff condition of simulated ore drawing was determined based on the principle of equal ore volume dilution ratio. The specific calculation process of the ore drawing cutoff condition is expressed as follows:

$$C_i = \frac{C_k}{W} \times W_k + \frac{C_y}{W} \times W_y \quad (8)$$

$$W = W_k + W_y \quad (9)$$

$$W_y = 1.67W_k \quad (10)$$

In this equation, according to the actual situation of the mine, C_i is the cutoff ore grade, 18%; C_k is the ore geological grade, 48%; C_y is the surrounding rock grade, 0; W_k is the current ore weight; and W_y is the current rock weight.

The ore is mined by free falling. Equation (10) can be obtained from Equations (8) and (9), when the ratio of the waste rock mass to the ore mass reached 1.67, the ore was stopped. The drawing process with sectional height and route spacing of 19 m × 20 m was selected as an example, as shown in Figure 4.

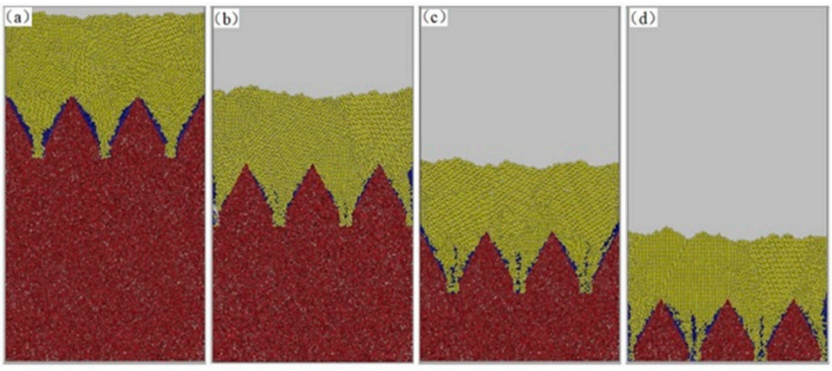

Figure 4. Numerical simulation of ore drawing process: (**a**) subparagraph 1; (**b**) subparagraph 2; (**c**) subparagraph 3; (**d**) subparagraph 4.

3.1.2. Analysis of Simulation Results

The ore drawing statistical results of 20 simulation schemes are shown in Table 2. From the statistical results of ore drawing in each sublevel, only the sublevel height × production drift spacing of 19 m × 20 m are presented as an example because of space limitations, as shown in Table 3.

Table 2. Statistical table of ore drawing results of each simulation scheme.

Analog Scheme	Segment Height/m	Approach Space/m	Difference between Recovery and Dilution Ratio/%
A 1	17.5	15	82.5
A 2		18	83.7
A 3		20	85.16
A 4		22	84.3
A 5	19	15	83
A 6		18	84.25
A 7		20	86.54
A 8		22	85.39
A 9	21	15	81.8
A 10		18	83.31
A 11		20	84.51
A 12		22	83.8
A 13	23.5	15	80
A 14		18	81.64
A 15		20	83.34
A 16		22	82.2
A 17	26	15	78.2
A 18		18	80.6
A 19		20	82.29
A 20		22	81.5

Table 3. Statistical data of 19 m × 20 m ore discharge results.

Discharge Section	Mine Release/ Mg	Total Release Ore /Mg	Total Release Ore /Mg	Recovery Ratio/%	Dilution Ratio/%
First segment	120.62	23.91	144.53	78.47	16.54
Second segment	225.56	25.91	251.47	105.61	10.30
Third segment	276.25	24.07	300.32	96.19	8.01
Fourth segment	206.12	23.81	229.93	97.18	10.35
Average	207.14	22.90	231.56	96.43	9.89

(1) Single-factor analysis

According to the numerical simulation drawing results, the single factor analysis of 20 schemes was carried out [30]. The difference between recovery and dilution ratio Y and sublevel height H and production drift spacing B is shown in Figure 5.

By analyzing the changing trend of the curve in Figure 5a, it can be seen that the difference between recovery and dilution ratio at each production drift spacing first increased and then decreased with the increase in sublevel height. The difference between recovery and dilution ratio when the production drift spacing was 20 m constantly remained the largest compared with other production drift spacings with the increase in sublevel height, indicating that the mining effect was optimal when the production drift spacing was 20 m, and the maximum value was 86.54% at the sublevel height of 19 m. The difference between recovery and dilution ratio increased from 85.16% to 86.54%, with a growth ratio of 1.62% and a small change when the production drift spacing was 20 m and the sublevel height increased from 17.5 m to 19 m, indicating that the values ranging from 17.5 m to 19 m were the appropriate sublevel heights.

By analyzing the changing trend of the curve in Figure 5b, it can be observed that the difference between recovery and dilution ratio at each sublevel height first increased and then decreased with the increase in production drift spacing. The difference between recovery and dilution ratio when the sublevel height was 19 m constantly remained the largest compared with other sublevel heights with the increase in production drift spacing, indicating that the stope had the best mining effect when the sublevel height was 19 m.

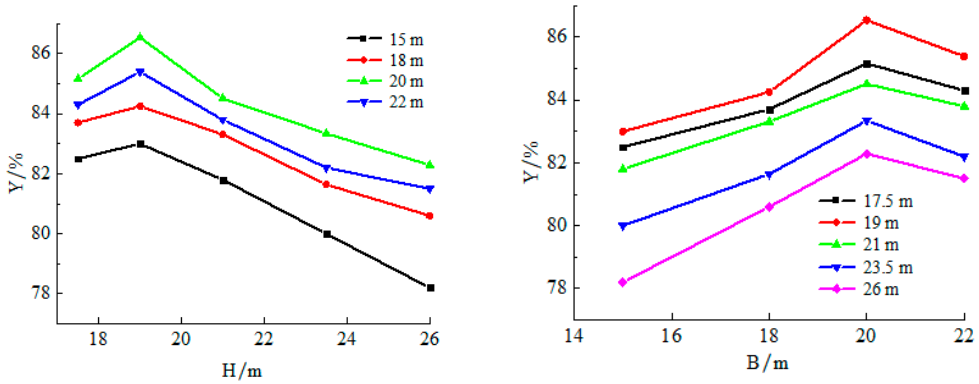

Figure 5. Relationship of the difference between recovery and dilution ratio Y and sublevel height H and production drift spacing B: (**a**) relationship curve of sublevel height H and the difference between recovery and dilution ratio Y; (**b**) relationship curve of production drift spacing B and the difference between recovery and dilution ratio Y.

(2) Comprehensive analysis

Table 2 demonstrates a quadratic polynomial with MATLAB (MathWorks, Natick, MA, USA), and the results are shown in Figure 6. The vertex of the surface in the figure was at a sublevel height of approximately 19 m, and the production drift spacing was approximately 20 m. The quadratic function relation of the difference between recovery and dilution ratio Y concerning sublevel height H and production drift spacing B can be obtained through fitting analysis, which can be expressed as:

$$Y = -0.13H^2 - 0.157B^2 + 5.594H + 6.517B - 0.018HB - 36.172 (R^2 = 0.8756) \quad (11)$$

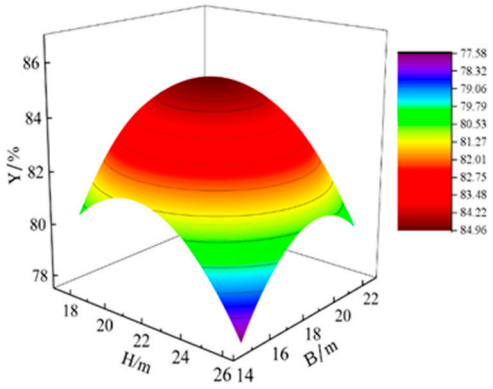

Figure 6. Relation curve of the difference between recovery and dilution ratio Y and sublevel height H and production drift spacing B.

In this fitting function, partial derivatives of H and B were calculated, and the maximum difference between recovery and dilution ratio was 84.15% when H = 20.18 m and B = 19.61 m. The results of theoretical calculation, numerical simulation, and function prediction are shown in Table 4.

Table 4. Statistical table of the range of structural parameters obtained by each method.

Bottom Structure	Theoretical Calculation	Numerical Simulation	Function Prediction
Segment height/m	17.5	19	20.18
Approach space/m	18.91~19.04	20	19.61

Combined with the occurrence of ore bodies (Figure 7) ranging from −500 m to −570 m, the changes in size and morphology of the ore body were large with the increase in sublevel height and production drift spacing. The edge of the ore body was difficult to control, resulting in a decrease in the ore recovery ratio and an increase in the dilution ratio. The sublevel height of 17.5 m in the development stage was defined as the mine design and was difficult to adjust. Thus, the sublevel height was kept constant at 17.5 m. As shown in Table 4, the optimal production drift spacing ranged from 18.91 m to 20 m. The crossing space of the −500 m level in the east of Chengchao Iron Mine is 60 m. The crossing space should be an integral multiple of the production drift spacing. The production drift spacing was set to 20 m based on the ellipsoid drawing theory [31] to ensure that the production drift spacing of the upper and lower sublevels formed a diamond layout. In particular, the optimal structure parameters of the stope were 17.5 m of sublevel height and 20 m of production drift spacing.

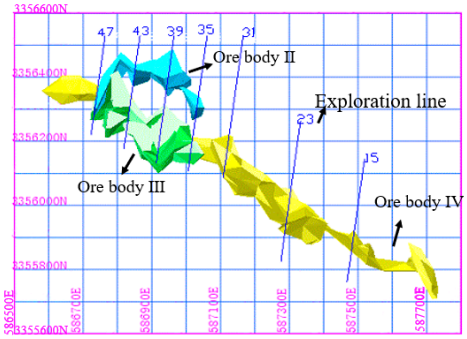

Figure 7. Top view of 3D visual model of No. II, III, and IV ore bodies from −500 m to −570 m.

3.2. Optimization of the Caving Step

3.2.1. Simulation Scheme

The interval of the caved ore of the stope was 3.0 m, and the caving step was approximately 4.0 m. For the simulation study, nine structural parameters, namely, 3.0, 3.5, 4.0, 4.5, 5.0, 5.5, 6.0, 6.5, and 7.0 m, were selected to determine the optimal caving step. The drawing model parameters are shown in Table 5, and the micromechanical parameters were the same as in Table 1.

Table 5. Macro model simulation parameter table.

Analog Number	Ore Height/m	Width/m	Caving Step/m	Current Cutoff Grade/%
B 1	33	20	3.0	18
B 2	33	20	3.5	18
B 3	33	20	4.0	18
B 4	33	20	4.5	18
B 5	33	20	5.0	18
B 6	33	20	5.5	18
B 7	33	20	6.0	18
B 8	33	20	6.5	18
B 9	33	20	7.0	18

Figure 8 shows the diagram of a single model of 17.5 m × 20 m. The actual drawing height was the sum of the sublevel and ridge heights formed through sublevel blasting. After the calculations, the actual drawing height was set to 33 m.

Figure 9 shows the initial diagram of the single model. The production drift direction is the *x*-axis, the vertical production drift is the *y*-axis, and the direction of the model height is the *z*-axis. The yellow particles are the overburden, the blue particles are the frontal waste rock, and the red particles are the ore. Under the action of the initial gravity field, the ore and rock flow from the lower ore discharge port to form recovery mining and stop when the cutoff grade is reached.

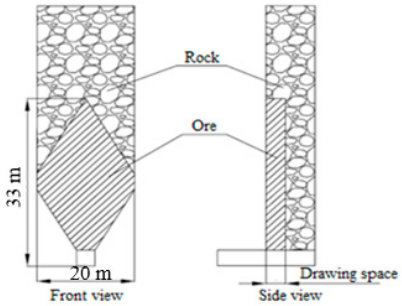

Figure 8. Single model design.

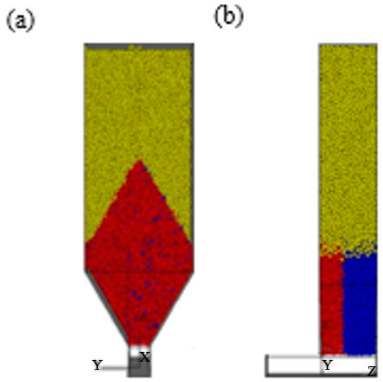

Figure 9. Initial diagram of the single model: (**a**) front view; (**b**) side view.

The cutoff grade of the 3D simulated ore drawing was the same as that of the 2D simulated ore drawing. Considering the model's limitations and shovel simulation, ore drawing in the three-dimensional single simulation experiment should be stopped when the mass ratio of waste rock and ore reaches 1.67 two consecutive times to ensure complete ore discharge.

3.2.2. Analysis of Simulation Results

Figure 10 shows the displacements of nine simulation schemes. The experimental results of each simulation scheme are shown in Table 6.

As shown in Figure 10a, the height of the drawn-out ore body increased with the increase in the caving step. The drawn-out ore body remained constant when the caving step reached 5.0 m, indicating that the height of the drawn-out ore body remained unchanged. The overall shape resembled an ellipsoid when the caving step increased to a certain degree.

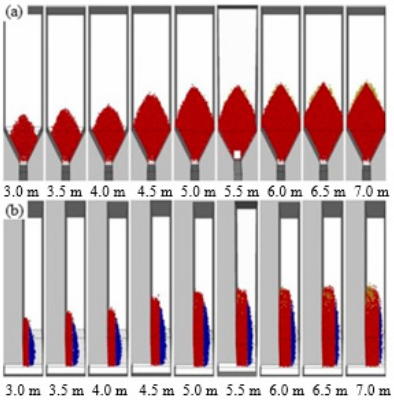

Figure 10. Schematic of the drawn-out ore body: (**a**) front view contrast of the drawn-out ore body; (**b**) side view contrast of the drawn-out ore body.

Table 6. Results of recovery indexes in the optimization simulation of caving step.

Analog Number	Caving Step/m	Recovery Ratio/%	Dilution Ratio/%	Difference between Recovery and Dilution Ratios/%
B 1	3	40.35	24.41	15.94
B 2	3.5	50.78	20.25	30.52
B 3	4	57.43	18.02	39.41
B 4	4.5	77.36	17.35	60.02
B 5	5	89.64	15.38	74.26
B 6	5.5	93.94	12.91	81.04
B 7	6	93.99	9.79	84.20
B 8	6.5	92.02	8.12	83.90
B 9	7	91.10	7.38	83.72

As shown in the analysis of Figure 10b, the thickness of the drawn-out ore body increased with the increase in the caving step. The thickness of red ore gradually increased, and the waste rock with the blue face slightly decreased. The body's morphology developed from "short and thick" to "long and thin" with the increase in the ore caving step.

As shown in Figure 10a,b, the morphology of the drawn-out ore body of each scheme resembled an ellipsoid, and the ore drawing process reflected the actual situation, indicating the rationality of the simulation study.

The ore recovery indexes, such as ore caving step, recovery ratio, dilution ratio, and the difference between recovery and dilution ratio, were obtained through sorting and summarizing. The data were fitted on MATLAB software (MathWorks, Natick, MA, USA), and the results are shown in Figures 11–13.

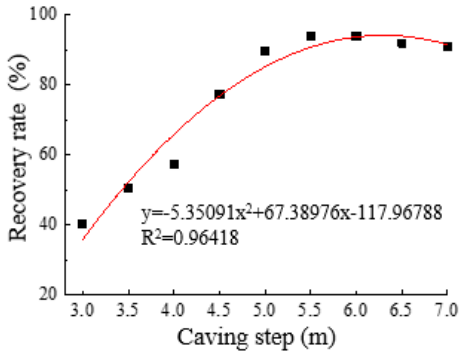

Figure 11. Relationship between ore recovery ratio and caving step.

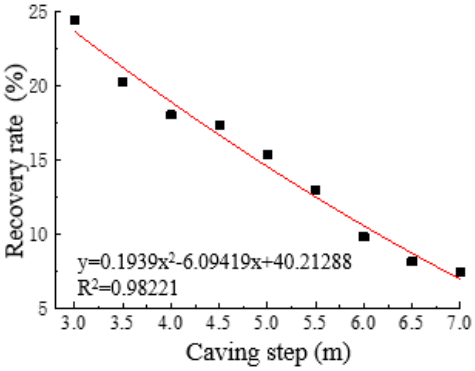

Figure 12. Relationship between ore dilution ratio and caving step.

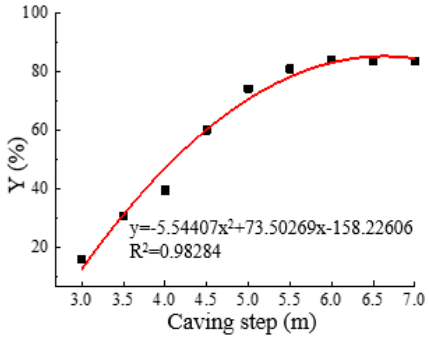

Figure 13. Relationship of the difference between recovery and dilution ratio Y and caving step.

(1) Recovery ratio

Figure 11 shows that the ore recovery ratio first increased and decreased with the increase in the caving step. The fitting curve results show that their relationship was quadratic, and the determination coefficient reached 0.96418. The recovery ratio was 40–60% when the caving step was 3–4 m, indicating that a large amount of waste rock in the front was mixed into the ore to intercept the normal outflow because of the small caving step, leading to premature dilution. The ore recovery ratio reached approximately 90% and remained unchanged when the ore drawing interval was 5–7 m. The recovery slightly declined when the caving step was 6 m, with an average reduction ratio of 1.55%. From the perspective of the fitting function, the recovery reached its maximum when the ore caving step was 6.3 m. Therefore, the recovery ratio showed that an ore caving step of 6–6.3 m was appropriate.

(2) Dilution ratio

As shown in Figure 12, the dilution ratio gradually decreased with the increase in caving step. The fitting curve results show that their relationship was quadratic, and the determination coefficient reached 0.98221. The dilution ratio was higher than 20% when the caving step was 3–3.5 m, indicating that a large amount of waste rock was mixed at this time, which would lead to an increase in mining production costs. The dilution ratio decreased to less than 10% when the caving step was 6–7 m, and the change was small. The average reduction ratio was 13.09%, indicating that the increase in waste rock mixing amount was less than that of the increase in total ore, leading to the decrease in dilution ratio. From the perspective of the fitting function, the dilution ratio was at its minimum value when the caving step was 15.71 m. Therefore, a caving step of 6–7 m was reasonable based on the dilution ratio.

(3) Difference between recovery and dilution ratio

The difference between recovery and dilution ratio is an important indicator for evaluating the effects of mining methods [32]. The greater the difference between the recovery and the dilution ratio, the better the economic effect. As shown in Figure 13, the difference between recovery and dilution ratio increased and decreased with the increase in the caving step. The fitting curve results show that their relationship was quadratic, and the determination coefficient reached 0.98284. The difference between recovery and dilution ratio gradually increased when the caving step was 3–6 m. The caving step was greater than 6 m, and the difference between recovery and dilution ratio showed a downward trend. From the perspective of fitting function, the difference between recovery and dilution ratio was at its maximum when the caving step was 6.63 m. Therefore, the appropriate range of the caving step was 6–6.63 m.

The appropriate range of the caving step of 6–6.3 m was obtained by considering the relationship between the recovery and the dilution ratio and the difference between the recovery ratio, the dilution ratio, and the caving step.

4. Experimental Study on Physical Ore Drawing

4.1. Experimental Scheme

In this experiment, the caving steps of 3.0, 4.0, 5.0, 6.0, and 7.0 m were taken under sublevel height and production drift spacing of 17.5 m × 20 m to conduct a simulation study of porous ore drawing. Appropriate suggestions were provided through thorough analysis and comparison of the experimental results.

The multi-segment three-dimensional ore drawing model was used in the experiment. According to the similarity theory, the stope structure parameters, ore and rock particles, and the total amount of ore and rock at the time of mining were simulated. The model size was length × width × height = 800 mm × 140 mm × 1100 mm. The experimental ore rock was Chengchao iron ore field ore rock. Compared with the field block, the particle size was ground at a 1:100 ratio, as shown in Figure 14a. The cross section of the drawing roadway was 38 mm × 36 mm (equivalent to 3.8 m × 3.6 m on site), and the roadway was arranged in a rhombic staggered arrangement. As shown in Figure 14b, the ore flowed downward by weight.

(**a**) Ore and waste rock particles (**b**) Physical drawing model framework

Figure 14. Physical ore drawing model. (**a**) Ore and waste rock particles; (**b**) Physical drawing model framework.

Each group of ore drawing test waste rock and ore was loaded at a 1:3 ratio, and three to four production drift roads were set for each sublevel. The ore drawing process is shown in Figure 15.

4.2. Results Analysis

As shown in Figure 15, the discharged bodies displayed a quasi-ellipsoid morphology and conformed to the ellipsoid theory, thereby confirming that this experiment was theoretically reasonable and feasible. The simulation experiment results of five ore caving steps of 3.0, 4.0, 5.0, 6.0, and 7.0 m were calculated under a sublevel height of 17.5 m and a production drift spacing of 20 m, as shown in Figure 16.

From Figure 16a,c, it can be seen that the variation trend of the recovery ratio and the difference between the recovery and the dilution ratio of the ore in each sublevel with different structural parameters were similar under the same ore drawing method. The residual bodies and recovery indexes in the discharged bodies gradually stabilized with the ore drawing sublevel. These findings indicate that each ore sublevel can be fully recovered under the existing structural parameters [33]. For the structural parameters of 17.5 m × 20 m × 5 m at sublevel II, the recovery ratio and the difference between recovery and dilution ratio were higher than the other structural parameters.

According to Figure 16b, the rock mixing ratio of each sublevel was significantly affected by the structural parameters under the same ore drawing method. Rock with structural parameters of 17.5 m × 20 m × 3 m had the highest mixing ratio. The actual caving step of the mine was approximately 3.5 m, indicating that the caving step of the stope should be increased at the same rate to optimize the recovery indexes.

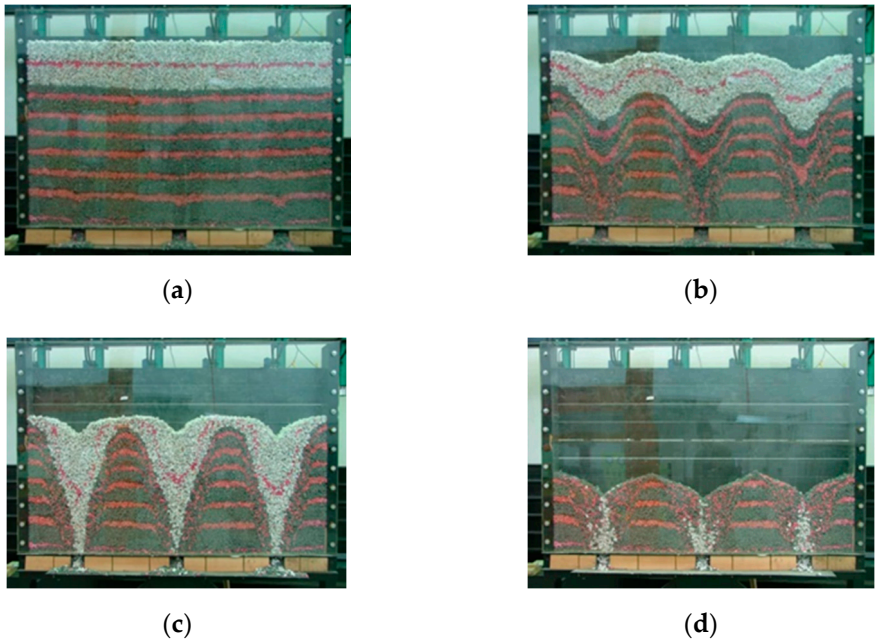

Figure 15. Drawing process diagram (**a**) before drawing, (**b**) at the initial drawing stage, (**c**) at the middle drawing stage, and (**d**) at the end of ore drawing.

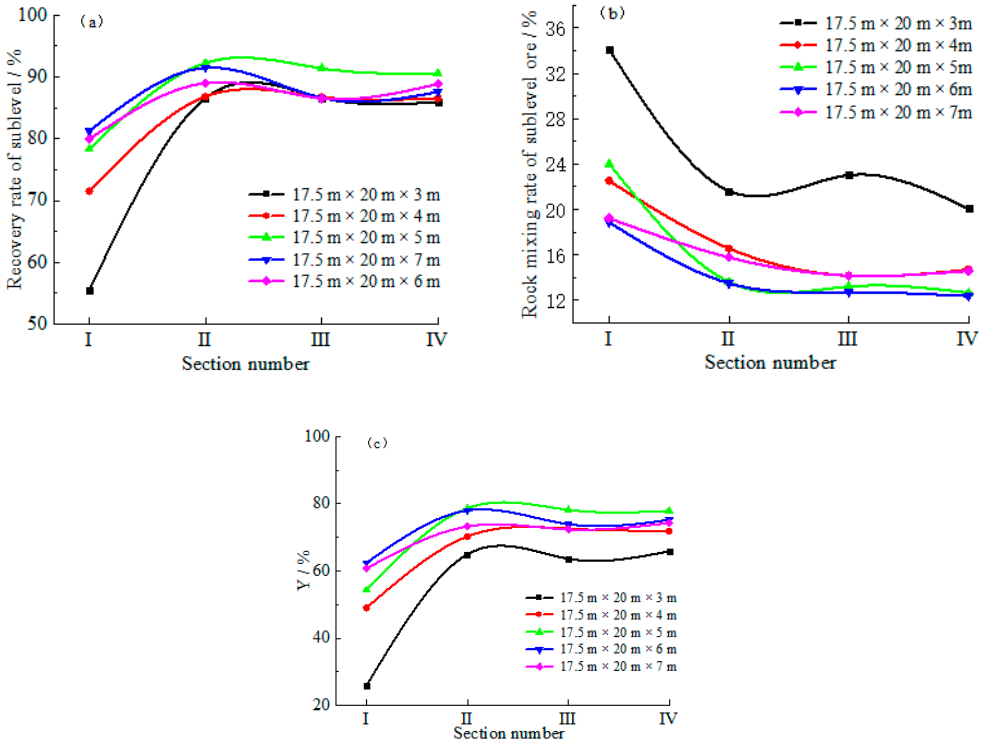

Figure 16. Curves of the recovery indexes of sublevel ore in each structural parameter scheme: (**a**) recovery ratio curve of sublevel ore; (**b**) rock mixing ratio curve of sublevel ore; (**c**) curve of the difference between recovery and dilution ratio of sublevel ore y.

Figure 17 presents the relationship between recovery indexes and ore interval drawing from an overall perspective without considering sublevels. The analysis of the curve showed that the dilution and ore recovery ratio first decreased and then increased. The change law of the difference between the recovery and the dilution ratio was similar to the recovery ratio when the caving step was 5.0 m. The maximum value of the difference

between the recovery and the dilution ratio was obtained. Therefore, the caving step of 5.0 m (loose coefficient of 1.3, equivalent to 3.8 m or so of the interval of caved ore) and the recovery effect were optimal when the sublevel height and production drift spacing were 17.5 m × 20 m, based on the difference between the recovery and the dilution ratio.

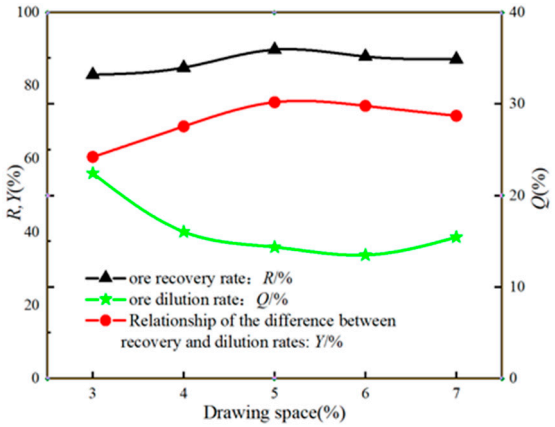

Figure 17. Relationship between recovery indexes and drawing space from an overall perspective.

4.3. Results Comparison between Numerical Simulation and Physical Experiment

PFC3D software (Itasca Consulting Group, Minneapolis, MN, USA) was used to conduct the numerical simulation research on nine drawing plans and the fitting analysis of each recovery index and ore drawing interval to determine the optimal caving step. A similar experiment of physical ore drawing in the laboratory was designed and combined with the theoretical calculation range of the caving step. The optimal caving step determined by each method is shown in Table 7.

Table 7. Various methods are used to obtain the optimal step range.

Bottom Structure	Theoretical Calculation	Numerical Simulation Research	Physical Similarity Simulation Experiment
Optimal caving step/m	4.46~6.07	6~6.3	5

Table 7 shows that the optimal caving step ranged from 6 m to 6.07 m through theoretical calculation and numerical simulation. The results only serve as a reference because similar physical experiments in practice inevitably involve human error. The optimal caving step, 6 m, was determined (extrusion blasting, loose coefficient of 1.3, equivalent to approximately 4.5 m of the interval of caved ore) by combining the actual effect of mine blasting.

5. Conclusions

In this paper, the sublevel caving method was studied through theoretical calculation, numerical simulation, and a laboratory test, and the following conclusions were drawn.

(1) The theoretical ranges of the optimal drift interval and caving step were calculated as 18.91~19.04 m and 4.46~6.07 m, respectively, based on the optimal arrangement and intersection degree of the discharged ellipsoid.

(2) Twenty groups of structural parameters were designed for simulation research. The binary quadratic function relation with sublevel height and production drift pace was fitted with the difference between the recovery and the dilution ratio as the objective function, on PFC2D software (Itasca Consulting Group, Minneapolis, MN, USA). The sublevel height and drift interval were 17.5 m × 20 m, based on the theoretical calculation results and the actual situation on site.

(3) The optimal caving step was investigated through a similar physical experiment and the theoretical calculation was performed on PFC3D software (Itasca Consulting Group, Minneapolis, MN, USA). The optimal caving step, 6 m, was determined through numerical simulation, physical experiment, and theoretical analysis.
(4) Through the optimization of bottom structure parameters, the loss and dilution of stope are effectively controlled, and energy consumption is significantly reduced. It is an effective measure for green mining and improves the production efficiency of the pillarless sublevel caving method.

Author Contributions: Conceptualization, Y.T. and M.G.; methodology, Y.T. and W.S.; software, M.G. and C.Z.; validation, Y.T., M.G. and Y.H.; formal analysis M.G.; investigation, Y.T.; resources, Y.T., data curation, M.G.; writing—original draft preparation, Y.T.; writing—review and editing, W.S.; visualization, Y.H. All authors have read and agreed to the published version of the manuscript.

Funding: This research was funded by the National Natural Science Foundation of China, grant number 52004019.

Institutional Review Board Statement: Not applicable.

Informed Consent Statement: Not applicable.

Data Availability Statement: Exclude this statement.

Acknowledgments: Financial support from the National Key R&D Program of China 2017YFC0602900 to the first author is gratefully acknowledged. The research is also partially supported by the Fundamental Research Fund for the Central Universities (FRF-TP-19-014A3). The authors would also like to thank Tan Y. Y. and Song W. D. for the discussions of the mining method.

Conflicts of Interest: The authors declare no conflict of interest.

References

1. An, L.; Xu, S.; Li, Y.H.; Peng, J. Optimization of rate of advance during ore breaking of caving method based on multi-method joint application. *Chin. J. Rock Mech. Eng.* **2013**, *32*, 754–759.
2. Liu, X.G.; Zhang, Z.T. Basis of Ore-drawing without Dilution for Sublevel Caving Method (First Part). *Metal Mine* **1995**, *11*, 5–9.
3. Wang, Y.P.; Yu, J. Optimization of breaking interval in non-pillar sublevel caving mining. *J. Cent. South Univ.* **2014**, *45*, 603–608.
4. Kaicheng, D.; Guihai, P.; Dan, H. Transition sublevel drawing optimization for large structural parameters of pillarless sublevel caving method. *China Min. Mag.* **2020**, *29*, 356–371.
5. Sun, G.; Lv, G. The development direction of no-pillar sublevel caving mining in China. *J. Inst. Technol.* **2007**, *29*, 4–6.
6. Brunton, I.D.; Fraser, S.J.; Hodgkinson, J.H.; Stewart, P.C. Parameters influencing full scale sublevel caving material recovery at the Ridgeway gold mine. *Int. J. Rock Mech. Min. Sci.* **2010**, *47*, 647–656. [CrossRef]
7. Jin, A.; Sun, H.; Wu, S.; Gao, Y. Confirmation of the upside-down drop shape theory in gravity flow and development of a new empirical equation to calculate the shape. *Int. J. Rock Mech. Min. Sci.* **2017**, *92*, 91–98. [CrossRef]
8. Yu, J. *Research on the Prediction of Ore Dilution and Loss Rate and the Optimization of Structural Parameters of High Sublevel Large Space Drive Interval Pillarless Sublevel Caving*; Center South University: Changsha, China, 2007.
9. Zhang, Z.G.; Liu, X.G.; Yu, G.L. *Bottom-Free Sublevel Caving Method without Depleted Ore Deposit: Non-Depleted Ore-Concentration Theory and Its Practice in Mines*; Northeastern University Press: Shenyang, China, 2007; pp. 6–7.
10. Kvapil, R. Gravity flow of granular materials in hoppers and bins. *Int. J. Rock Mech. Min. Sci.* **1965**, *2*, 35–41. [CrossRef]
11. Janelid, I.; Kvapil, R. Sublevel caving. *Int. J. Rock Mech. Min. Sci.* **1966**, *3*, 129–153. [CrossRef]
12. David, J. Computer simulation of the movement of ore and waste inan underground mining pillar. *Can. Min. Metall. Bull.* **1968**, *61*, 854–859.
13. Xu, S.; An, L.; Feng, X.T.; Dong, J.K.; Li, Y.H. Research on granular flow laws of caved ore and rock for steeply dipping thin vein. *J. Min. Saf. Eng.* **2013**, *30*, 512–517.
14. Xu, S.; An, L.; Li, Y.H.; Dong, J.K.; Li, Y.H. Optimization of caving space for different angles of end-wall during pillarless sublevel caving. *J. Northeast. Univ. Nat. Sci.* **2012**, *33*, 120–123.
15. Li, X.; Sheng, J.; Cheng, A.; Huang, Z. Study on structural parameter for non-pillar sublevel caving. *Ind. Miner. Process.* **2011**, *40*, 21–23.
16. Guo, H.; He, Z.; Zhang, Z.; Su, H.; Zhu, Q. Influence analysis of stope structure parameters on the drift stability in non-pillar sublevel caving under backfill. *Min. Res. Dev.* **2020**, *40*, 12–18.
17. Wu, A.; Wu, L.; Liu, X.; Sun, X.; Zhou, Y.; Yin, S. Study on structural parameters of sublevel caving. *J. Cent. South Univ.* **2012**, *43*, 1845–1850.

18. Zhao, Y.; Chen, Y.; Li, C.; Chen, J. Research on structural parameter optimization of sub level caving method. *Ind. Miner. Process.* **2019**, *48*, 16–21.
19. Jin, A.; Sun, H.; Meng, X.; Gao, Y.; Wu, Q.; Zhang, G. Study of best caving steps under different ore methods of sublevel caving. *J. Cent. South Univ.* **2017**, *48*, 3037–3043.
20. Tao, G.; Lu, M.; Zhang, X.; Zhang, R.; Zhu, Z. A new diversion drawing technique for controlling ore loss and dilution during longitudinal sublevel caving. *Int. J. Rock Mech. Min. Sci.* **2019**, *113*, 163–171. [CrossRef]
21. Li, T.; Fu, J.X.; Song, W.D. Study on law of surrounding rock movement induced by mining large and thick ore body. *J. Min. Saf. Eng.* **2018**, *35*, 978–983.
22. Fu, J.X.; Du, J.H.; Tan, Y.Y. The falling process and mechanism of concealed gob roof during the caving mining of the gently inclined heavy ore. *J. Min. Saf. Eng.* **2017**, *34*, 891–898.
23. Meng, Q.B.; Wang, C.K.; Han, L.J. Analysis on stope surrounding rock stability and mining entrance repair technology in sublevel caving method. *J. Min. Saf. Eng.* **2019**, *36*, 364–372.
24. Jin, C.; Dong, Z.M.; Gong, S.G. Study on the enlarged-structure parameters of sublevel caving in Meishan Iron Mine. *Metal Mine* **2000**, *4*, 17–19.
25. Huang, Z.; Sheng, J.L.; Li, X. Parametric analysis of high-segment and large-pitch structural parameters of sublevel caving without pillars. *Min. Technol.* **2011**, *11*, 11–12.
26. Zhu, H.C. PFC and application case of caving study. *Chin. J. Rock Mech. Eng.* **2006**, *25*, 1927–1931.
27. Zhou, C.B.; Yao, Y.K.; Guo, L.W.; Yin, X.P.; Fan, X.F.; Shang, Y. Numerical simulation of independent advance of ore breaking in the non-pillar sublevel caving method. *J. China Univ. Min. Technol.* **2007**, *17*, 295–300. [CrossRef]
28. Itasca Consulting Group Inc. *Particle Flow Code (Version 3.0)*; ICG: Minneapolis, MN, USA, 2004; pp. 22–26.
29. Brady, B.H.G.; Brown, E.T. *Rock Mechanics for Underground Mining*; Allen & Unwin: London, France, 1985; pp. 334–339.
30. Zhao, Y.L.; Cheng, Y.M.; Li, C.; Chen, J. Structural parameters optimization of sublevel caving method without pillars based on PFC3D. *Nonferrous Met. (Min. Sect.)* **2019**, *71*, 10–16.
31. Wang, C.H. *Theory of Ore Flow*; Metallurgical Industry Press: Beijing, China, 1982; pp. 5–10.
32. Zhang, H.F.; Chi, X.W. Application of particle flow method in structural parameter optimization of sublevel caving method without bottom column. *Min. Technol.* **2018**, *18*, 19–22.
33. Tan, B.H.; Zhang, Z.G.; He, R.X.; Zhu, Q. Discussion on the rationality and experimental research of the ore-drawing ellipsoid arrangement theory. *J. Northeast. Univ. Nat. Sci.* **2019**, *40*, 1014–1019.